Special Feature: Recent Research Developments on Periodic Mesoporous Organosilicas

Research Report

Computational Studies on the Intermolecular Interactions of Bridging Organic Groups in Periodic Mesoporous Organosilica

Soichi Shirai

Report received on Apr. 16, 2019

ABSTRACT Bridging organic groups of periodic mesoporous organosilica (PMO) materials are densely distributed in the pore walls and are in proximity to each other. This unique structure induces intermolecular electronic interactions of organic groups that play a crucial role in the functionalities of the material. Theoretical calculations have been effectively combined with experimental analyses to clarify the details of these interactions. In this article, our studies on the excimers of the organic groups and the electron transfer between the metal complexes formed on the pore surfaces of bipyridine-bridged PMO (BPy-PMO) are briefly reviewed. Typical aromatic excimers were initially examined to explore an adequate computation scheme. Cyclophane derivatives were subsequently studied as the models of the organic groups. The calculation results on a paracyclophane with benzene rings connected by $SiMe_2$−O−$SiMe_2$ chains were consistent with the experimental results of benzene-bridged PMO. The distribution of the metal complexes on the pore surfaces of BPy-PMO was examined by Monte Carlo simulation. The results implied that the adjacent pair of photosensitizer and photocatalyst complexes might be the active center of CO_2 reduction. The results of quantum chemical calculations adopting a cluster model of the active center suggested a mechanism with a through Si−O−Si bond electron transfer.

KEYWORDS Mesoporous Organosilica, Intermolecular Interaction, Excited State, Aromatic Excimer, Electron Transfer, Ab Initio Quantum Chemical Calculation, Computational Simulation

1. Introduction

Periodic mesoporous silica (PMO) materials are synthesized by the poly-condensation of organosilane precursors having the formula R−{Si(OR')$_3$}$_x$ (R: organic bridging group, R': Me, Et, *i*Pr, etc., and $x \geq 2$) in the presence of a template surfactant.[1-8] Thus, various electronic properties and functionalities that originate from R can be introduced into the pore walls.[9,10] This versatility is a primal advantage of PMO materials, in addition to their uniform porous structure.

The bridging organic groups, which are covalently connected to the silica framework, are densely introduced into the pore walls and are in proximity to each other. This unique structure induces electronic interactions that originate from the overlap of the wavefunctions of the organic groups. The interactions have the potential to induce electronic properties and phenomena that are absent in isolated molecules. The most typical example is the formation of an excimer (excited dimer), as suggested by the appearance of a significantly red-shifted, broad, and emission band without vibrational fine structure. Excimer fluorescence upon photoexcitation is commonly observed in PMO materials, although there are some exceptions.[11-15] The overlap of the wavefunctions also enables carrier transfers between the organic groups. A three-armed phenylenevinylene-bridged PMO was developed as a first hole-transporting material with mesochannels.[16] A 4,7-dithienyl-2,1,3-benzothiadiazole (DTBT)-bridged PMO was subsequently synthesized as a hole-transporting PMO with visible-light absorbance. The thin film of DTBT-PMO acts as a hole-transporting layer in organic solar cells by filling an n-type material into the mesopores.[17] For these materials, carrier transfer along the π-stacking direction is assumed. In contrast, for a PMO with 2,2'-bypiridine-bridging groups (BPy-PMO),[18] electrons are considered to transfer between the metal complexes formed on the pore surfaces through the silica framework.[19,20]

Thus, electronic interactions between the organic groups are closely related to the very basis of the properties and functionalities in PMOs, and therefore

should be clarified in detail. However, the electronic interactions are based on the wavefunctions and microscopic molecular structures; therefore, experimental studies alone would not be adequate. We have thus conducted theoretical studies that utilize computational methods and combined them with an experimental approach. Some of our studies on the intermolecular interactions in PMO materials are reviewed in this article.

2. Excimer Fluorescence

When a PMO material with excimer fluorescence is utilized in photoemissive devices, the wavelength of its fluorescence emission should be adjusted in accordance with its use. In a light-harvesting system that employs a PMO as its antenna unit, the photoenergy transfers from the photoexcited organic groups to the acceptor molecules situated in the mesopores.[13,21-24] A larger overlap between the emission band of the donor and the absorption band of the acceptor results in a higher rate of resonance energy transfer. In the case where the excimers of the organic group act as the energy donors, the overlap between the absorption and emission bands should be maximized by adjustment of the excimer fluorescence energy. Thus, computational predictions of the excimer fluorescence energies from quantum chemical methods should be pursued for the theoretical design of such materials.

Aromatic excimers have been theoretically studied for more than half a century since their discovery.[25] However, ab initio quantum chemical calculations of aromatic excimers have only recently been examined, mainly because of their large system size and the complexity of the excited states of aromatic molecules. Therefore, appropriate calculation methods continue to be explored. In this context, we have calculated typical aromatic excimers to find an adequate calculation scheme.[26] Cyclophane derivatives were subsequently calculated as models of PMO organic groups that interact with each other in the pore walls.[27]

2. 1 Systematic Calculations of Aromatic Excimers

Aromatic excimers are dimeric species of aromatic molecules that are stable only in the excited states. A schematic diagram of the ground and excited state potential energy curves of an aromatic dimer against the intermolecular distance r(R−R), is shown in **Fig. 1**.[28] The attractive interaction in the excited state is much stronger than that in the ground state where a weak interaction originated from the dispersion force is dominant. Hence, the two aromatic molecules are more strongly bound in the excited state than in the ground state, and the equilibrium intermolecular distance in the excited state r_e, is located in the repulsive region of the ground state curve. Thus, the energy difference between the ground and excited states at r_e becomes extremely small. This is the mechanism for the red-shift of the fluorescence emission, the most conspicuous feature of the excimer. The excimer fluorescence energy can be estimated by calculating these potential energy curves.

The strong attractive interactions in the excited state are caused by the mixing of exciton resonance (ER) and charge resonance (CR).[29] ER corresponds to the interaction between the transition dipole moments derived from the intramolecular excitations. In contrast, CR is the Coulombic interaction that arises from the intermolecular excitations. Assuming that the excimeric state is originated from a single excitation from the highest occupied molecular orbital (HOMO) to the lowest occupied molecular orbital (LUMO) of the monomer, electron configurations that are relevant to the ER and CR can be represented based on the monomer orbitals, as shown in **Figs. 2**(a) and (b). The dimer orbitals are the linear combinations of

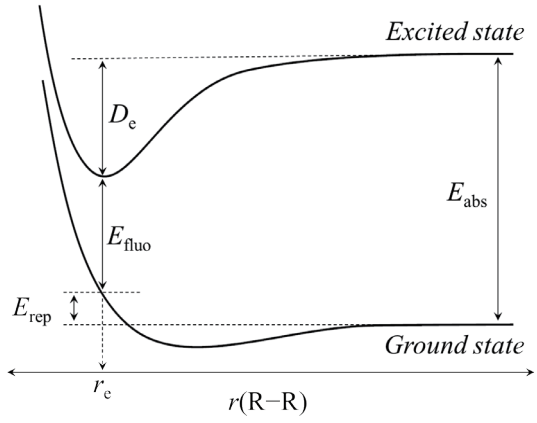

Fig. 1 Schematic diagram of the potential energy curves of the ground and excited states of an aromatic dimer with the intermolecular distance r(R−R). The parameters indicated are the absorption energy (E_{abs}), fluorescence energy (E_{fluo}), equilibrium intermolecular distance in the excited state (r_e) and excimer binding energy (D_e).

monomer orbitals (Fig. 2(c)); therefore, the electron configurations that are required to describe ER and CR can be represented using dimer orbitals H_D-1, H_D, L_D and L_D+1 (Fig. 2(d)). These are the main configurations of the excimeric state. To calculate the excited state curve of the aromatic dimer precisely, the contributions of these configurations and the dynamical electron correlation should both be adequately incorporated. There requirements could be met by employing the multiconfiguration quasi-degenerate second order perturbation theory method (MCQDPT).[30] Here, MCQDPT is one of the most successful and widely used multireference perturbation theory methods. The MCQDPT adopts the complete active reference space (CAS), which consists of all electron configurations generated by distributing the active electrons to the active orbitals. Although the calculation accuracy improves by an increase of the number of active electrons and orbitals, the dimension of the CAS exponentially increases with these parameters. In this study, the naphthalene, anthracene, pyrene and perylene dimers were systematically calculated by selecting four dimer π orbitals, H_D-1, H_D, L_D, and L_D+1, and four π electrons as active orbitals and electrons, respectively. The adopted CAS can be denoted as CAS(4πe, 4πo). The benzene dimer was additionally calculated using MCQDPT with CAS(12πe, 12πo).

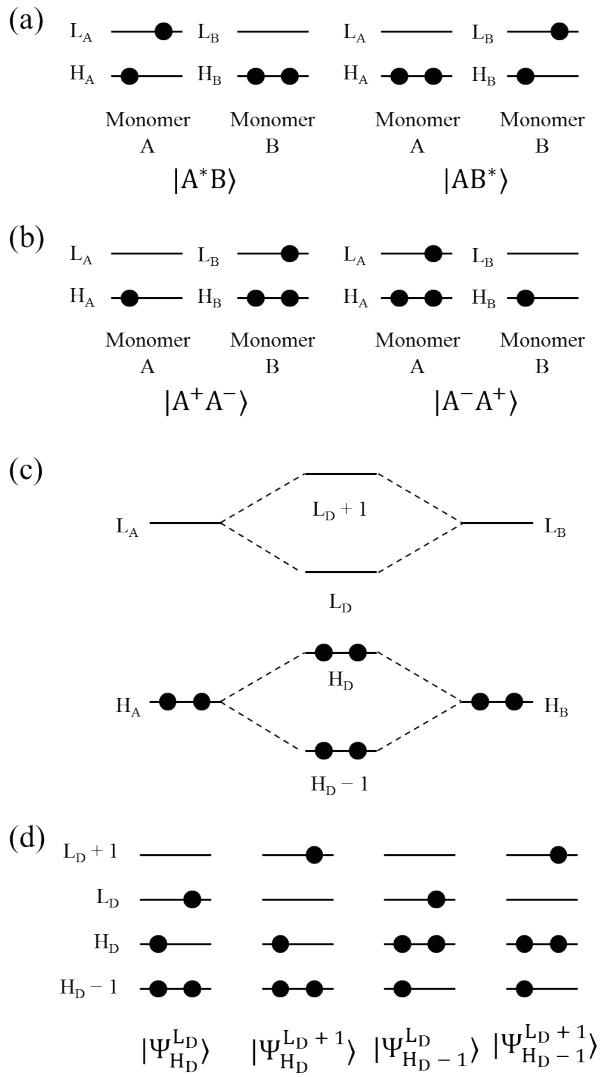

Fig. 2 Singly-excited configurations in the framework of monomer and dimer orbitals. HOMO−1, HOMO, LUMO, and LUMO+1 are denoted by H−1, H, L, and L+1 with A, B, and D subscripts representing monomers A and B, and the dimer, respectively. Electron configurations representing (a) the exciton resonance (ER), and (b) the charge resonance (CR). (c) Four dimer orbitals derived from interactions between the frontier orbitals of monomer A and B, and (d) singly-excited configurations in the dimer orbitals.

The calculations were performed as follows. First, the molecular structures of the monomers were optimized using density functional theory (DFT) with the B3LYP functional.[31,32] The dimer models with eclipsed parallel configurations were constructed by superimposing a monomer onto another monomer. The potential energy curves for the ground state (S_0) and the excited state (S_1) were calculated by the MCQDPT method as a function of the intermolecular distance r(R−R), from 2.7 to 10.0 Å. Molecular geometrical optimizations were conducted using Gaussian 03,[33] while the MCQDPT calculations were performed using GAMESS.[34] Here, the results using the 6-31G(d) basis set[35,36] are presented. The basis set dependence is also examined in Ref. (26).

The calculated potential energy curves are presented in **Fig. 3**. The excited state curves are more attractive than those of the ground state, and their minima are located in the repulsive region of the ground state curves, as illustrated in Fig. 1. The excimer fluorescence energies (E_{fluo}) obtained from these curves are in good agreement with the available experimental values (**Table 1**).[37-41] The absorption energies (E_{abs}) obtained from the curves at r(R−R) = 10.0 Å are also close to the corresponding experimental values, which indicates that the ground and excited state energies are evaluated in a balanced manner for the entire region. The results demonstrate that the E_{fluo} and E_{abs} energies, and other spectroscopic parameters, can be precisely

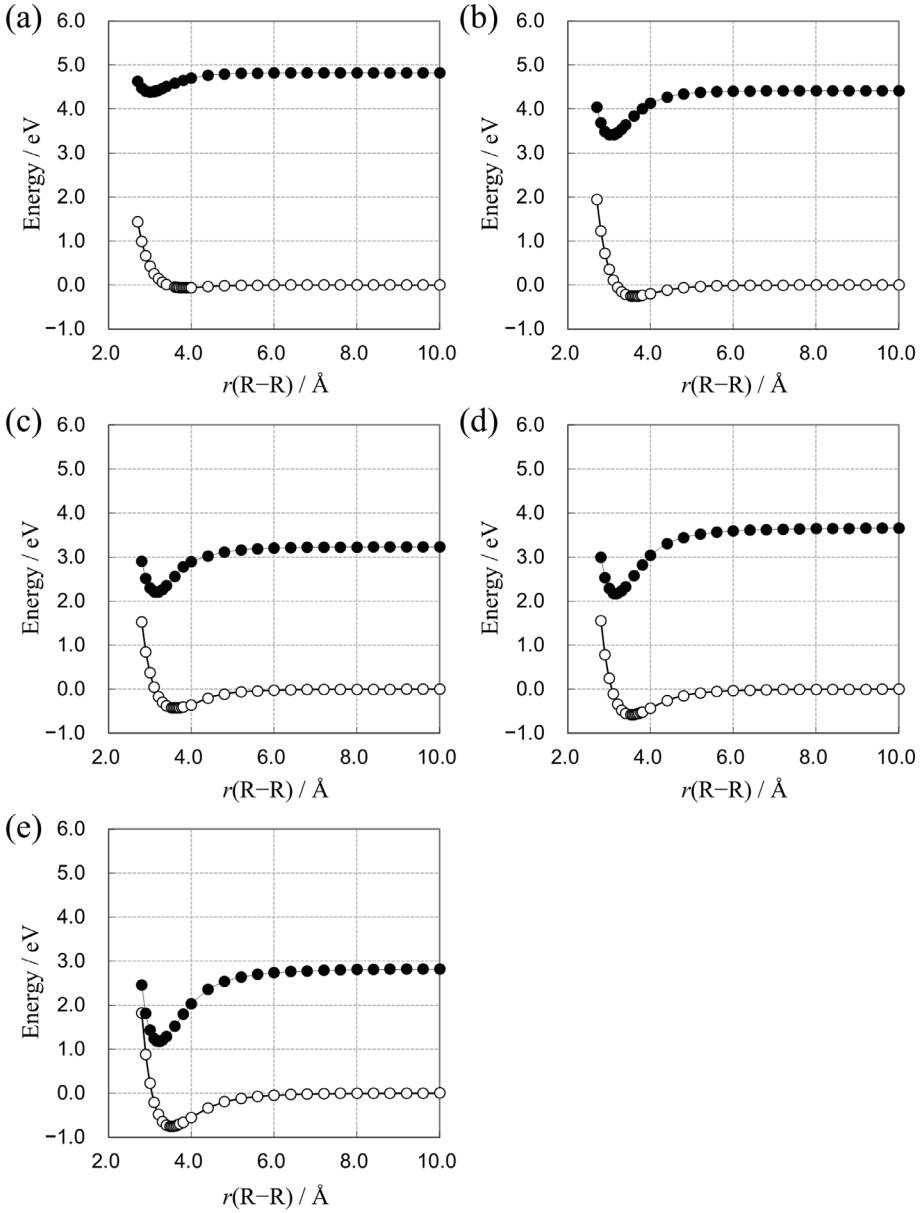

Fig. 3 Potential energy curves of the ground (○) and excited states (●) of the (a) benzene, (b) naphthalene, (c) anthracene, (d) pyrene, and (e) perylene dimers. The excited state curves are correlated to the L_b (B_{2u}) dissociation channel in the benzene dimer, and to the L_a channel in the other dimers.

Table 1 Calculated intermolecular equilibrium distance (r_e), excimer binding energy (D_e), fluorescence energy (E_{fluo}) and absorption energy (E_{abs}) of the benzene, naphthalene, anthracene, pyrene and perylene excimer states. Available experimental values are also presented.

Excimer	r_e (Å)	D_e (eV)	E_{fluo} (eV)		E_{abs} (eV)	
			Calc.	Exp.	Calc.	Exp.
$(benzene)_2$	3.00	0.44	3.96	3.94[37]	4.82	4.79[38]
$(naphthalene)_2$	3.05	1.00	3.17	3.13[37]	4.41	4.45[39]
$(anthracene)_2$	3.15	1.02	2.28	2.30[40]	3.23	3.27[37]
$(pyrene)_2$	3.16	1.49	2.42	2.59[37]	3.66	3.70[37]
$(perylene)_2$	3.21	1.65	1.69	1.94[41]	2.82	2.86[37]

estimated by the MCQDPT calculation with the CAS including the main configurations (Fig. 2(d)). The calculation scheme was then applied to the cyclophane derivatives (Sec. 2. 2).

In the naphthalene and pyrene monomers, the L_a excited state originated from the HOMO−LUMO excitation is the second lowest excited state (S_2), and the lowest excited state (S_1) is the L_b excited state, which is different from the L_a state.[42,43] It has been experimentally suggested that the fluorescence emissions of the naphthalene and pyrene excimers are derived from the L_a-derived states. Therefore, the ordering of the energy levels of L_a-derived and L_b-derived dimer states changes depending on r(R−R): $L_a > L_b$ when r(R−R) is long, while $L_a < L_b$ when r(R−R) is short. In Ref. (26), the L_a-derived states are focused on as excimeric states and the L_b-derived states are ignored, except for the benzene dimer; the excimer fluorescence of the benzene dimer is originated from the L_b-derived state. The inversion of the L_a-derived and L_b-derived excited states in the naphthalene dimer during excimer formation was further studied using the advanced multireference theory based on the density matrix renormalization group.[42]

2. 2 Calculations of Cyclophane Derivatives as the Models of PMO Organic Groups

The aromatic excimer is a short-lived excited complex; therefore, experimental analysis of its molecular structure and electronic states is a challenging subject. Molecular interaction in the condensed phase is also dominantly affected by the surrounding environment. Study using a simplified model system is therefore helpful for detailed analysis. In this context, cyclophane derivatives in which two aromatic molecules are connect by molecular chains and fixed in a face-to-face configuration have been traditionally employed in the study of aromatic molecular interactions.[44-48] [2,2]PCP (**Fig. 4**(a)) and [3,3]PCP (Fig. 4(b)), where PCP represents paracyclophane, are the most typical examples synthesized in the earliest period of the field and have been extensively studied. The electronic states of cyclophane derivatives are featured by transannular interactions between the aromatic moieties and the effects of the bridging chains. Thus, the Si−O−Si bridged cyclophane derivatives are expected to be ideal models of PMO organic groups that interact with each other in the pore walls. The ground and excited states of SiPCP (Fig. 4(c)) were calculated, and compared with [2,2]PCP and [3,3]PCP.[27] Here, the results for SiPCP are reviewed.

An analytical gradient calculation for MCQDPT is not implemented in commonly-available programs. The potential energy curves of the benzene dimer were thus calculated using MCQDPT, MP2, and time-dependent DFT (TDDFT) methods to explore alternative optimization schemes. The calculated curves are plotted in **Fig. 5**; the curves from MP2 and TD-B3LYP are shifted so that their energy levels at r(R−R) = 10.0 Å are the same as the corresponding MCQDPT values. The ground state curve calculated

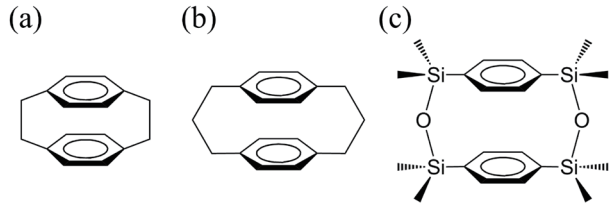

Fig. 4 Structures of (a) [2,2]paracyclophane ([2,2]PCP), (b) [3,3]paracyclophane ([3,3]PCP), and (c) siloxane-bridged paracyclophane (SiPCP). In this article, the results of SiPCP are reviewed (see text).

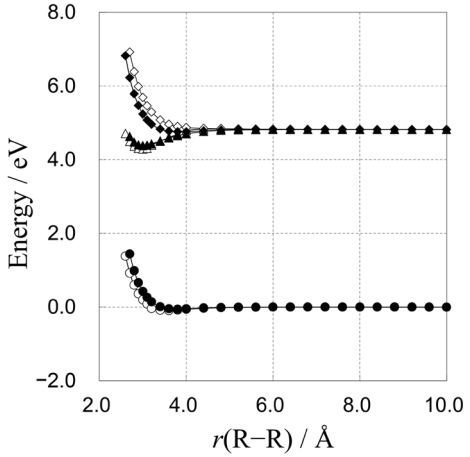

Fig. 5 Potential energy curves for the A_{1g} ground state (MCQDPT (●) and MP2 (○)), and the $^1B_{1g}$ (MCQDPT (▲) and TD-B3LYP (△)) and $^1B_{2u}$ (MCQDPT (◆) and TD-B3LYP (◇)) excited states of the benzene dimer as a function of the intermolecular distance, r(R−R).

with MP2 is close to that calculated with MCQDPT. The shapes of the excited state curves of TD-B3LYP are similar to those of MCQDPT. On the basis of this assessment, the molecular structures of SiPCP for the ground state (S_0) and the excited state (S_1) were optimized using MP2 and TD-B3LYP, respectively. The electronic structure of the ground and excited states at their optimized geometries were then calculated using MCQDPT with the CAS(12πe, 12πo) reference space. The basis set used was 6-31G(d).[35,36,49] Note that the attractive intermolecular interaction originated from the dispersion force is not incorporated by TDDFT, while it is considered by MCQDPT. Nevertheless, the TD-B3LYP calculations give the potential energy curves that are similar to those obtained with MCQDPT. The influence of the absence of dispersion force may be small because of the small molecular size of the benzene monomers, or is partially canceled by other factors. The validity of TDDFT calculations in the studies of other aromatic excimers should thus be carefully examined.

Although there are two conformers of SiPCP, boat and chair, the results of the boat conformer are discussed here because the results of these conformers were very similar. The optimized structures are shown in **Fig. 6**. The two benzene rings are in a slipped parallel configuration with the intermolecular distance between the benzene rings r_{ph-ph}, of 3.53 Å in S_0 (Fig. 6(a)), while they are in an eclipsed parallel configuration with r_{ph-ph} of 3.16 Å in S_1 (Fig. 6(b)). The results suggest a change of the dominant intermolecular interactions and the arrangement of the PMO organic groups upon excimer formation. The benzene rings of SiPCP are almost planar, even in the ground state, in contrast to those in [2,2]PCP and [3,3]PCP.[26] The calculated excitation energies and oscillator strengths are summarized in **Table 2**. In the structure optimized for the S_0 state, the energy difference between S_1 and S_2 is negligibly small. In contrast, with the structure optimized for the S_1 state, the energy levels of S_1 and S_2 are largely split because of a decreased r_{ph-ph}. These behaviors are consistent with the potential energy curves of the benzene dimer (Fig. 5). From the perspective of ER, the transition dipole moments of two benzene rings are anti-parallel and parallel in the S_1 and S_2 states, respectively, which results in oscillator strengths that are in the order of $S_2 > S_1$. The oscillator strengths in S_1 are almost zero; therefore, the absorption band can be assigned to the $S_0 \rightarrow S_2$ transition at the geometry optimized for S_0, while the fluorescence emission band is assigned to the $S_1 \rightarrow S_0$ transition at the geometry optimized for S_1, according to Kasha's rule. The calculated absorption (E_{abs}) and fluorescence emission (E_{fluo}) energies are in good agreement with the experimental values, and are also close to those of Ph-PMO; E_{abs} and E_{fluo} of Ph-PMO are 4.59 eV and 3.65 eV, respectively. The energies are both approximately 0.3 eV lower than that of the benzene dimer. The lowering of these energies could be attributed to the effects of $SiMe_2$−O−$SiMe_2$ bridging chains based on the calculation results of the benzene and substituted benzene monomers.

In conclusion, cyclophane derivatives in which the aromatic molecules are connected by Si−O−Si bridging chains are useful model compounds in the study of molecular interactions of PMO organic groups. With regard to the excimer fluorescence, the interaction between two organic groups is dominant.

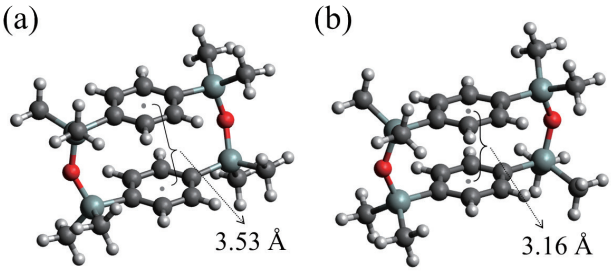

Fig. 6 Molecular structures of boat SiPCP optimized for (a) the ground state and (b) the S_1 excited state. The ring-ring distances (r_{ph-ph}) are shown.

Table 2 Calculated transition energies and oscillator strengths of boat SiPCP. Available experimental values are also given.

Molecular geometry	Excited state	Excitation energy (eV)		Oscillator strength
		Calc.	Exp.[27]	
optimized for S_0	S_1	4.63		0.0001
	S_2	4.69	4.56	0.0030
optimized for S_1	S_1	3.83	3.63	0.0000
	S_2	4.51		0.0057

3. Electron Transfer between Metal-complexes Formed on the Pore Surfaces of BPy-PMO

BPy-PMO, which enables metal complex formation on the pore surfaces, is expected to be a promising platform for functional materials such as catalysts and photocatalysts.[18] The immobilization of homogeneous complexes may allow ease of separation from reaction solutions, for recovery and reuse. Porous structures having high surface areas and large pores are also advantageous for catalytic reactions with high efficiency.

Ru(PS)-Ru(Cat)-BPy-PMO is a recently synthesized CO_2 reduction photocatalyst in which $[Ru(bpy)_3]^{2+}$ and $Ru(bpy)(CO)_2Cl_2$ are formed on the BPy-PMO pore surfaces.[19] In this system, $[Ru(bpy)_3]^{2+}$ (Ru(PS)) acts as a photosensitizer for visible light activation and photoexcited electron transfer from Ru(PS) to $Ru(bpy)(CO)_2Cl_2$ (Ru(Cat)), which functions as the CO_2 reduction catalyst. Photoelectron transfer occurs via the overlap of donor and acceptor wavefunctions. The wavefunction overlap is rapidly reduced with an increase in the distance between the donor and acceptor; therefore, the molecular motion that enables complexes to approach to each other play an important role in efficient electron transfer in a homogeneous environment. However, the metal complex formed on BPy-PMO is fixed on the pore surface because the bpy ligand is the BPy-PMO organic groups that are connected to the silica framework with Si−C bonds. Thus, it could be expected that electron transfer from Ru(PS) to Ru(Cat) occurs in Ru(PS)−Ru(Cat) pairs in which these complexes are fixed in proximity to each other. The distribution of the complexes in the mesochannels was next studied theoretically by Monte Carlo simulations. The bpy organic group, Ru(PS) and Ru(Cat) are modeled as spheres B, P and C, respectively. First, one of the BPy-PMO mesochannels was modeled as a hollow hexagonal cylinder (**Figs. 7**(a) and (b)). The cylinder was constructed by stacking 332 equilateral hexagonal rings and each ring consists of 30 B spheres. The array of B spheres represents the ordered structure of the BPy-PMO pore wall (Fig. 7(c)). Second, B spheres were substituted at random by P or C spheres with specified probabilities (Fig. 7(d), **Table 3**). Finally, the numbers of P spheres (N_P), C spheres (N_C) and the P−C sphere pairs (N_{CP}) were counted. The simulation was executed 100 times and N_P, N_C and N_{CP} were totaled in each. The pore wall of BPy-PMO consists of multiple bipyridine-silica layers, so that the molar ratios of complexes on the pore surfaces are higher than their total molar ratios. The probabilities for replacements were then set to be 1.5 times greater than the molar ratios, x and y, assuming a three-layered pore wall. Here, x and y are molar ratios for Ru(PS) and Ru(Cat), respectively. In the substitution process, P−P, P−C and C−C in the same ring were separated by at least one B sphere in the substitution step. This restriction was adopted because bulky complexes could be separated by at least one bpy moiety along with the bpy π-stacking direction. Thus, C adjacent to P corresponds to Ru(Cat) connected to Ru(PS) via Si−O−Si. As shown in Table 3, the N_{CP} values are consistent with the activity of photochemical CO_2 reduction. The results strongly suggest that the photosensitizer−catalyst pair is the possible active center of the photocatalysis.

Ru-Re-BPy-PMO, in which $[Ru(bpy)_3]^{2+}$ and $Re(bpy)(CO)_3Cl$ are immobilized on the pore surfaces of BPy-PMO, is another recently-developed CO_2 reduction photocatalyst.[20] Ru-Re-BPy-PMO exhibits higher photocatalytic activity than Re-BPy-PMO which has only $Re(bpy)(CO)_3Cl$, and this suggests a photosensitizing effect of $[Ru(bpy)_3]^{2+}$ and the

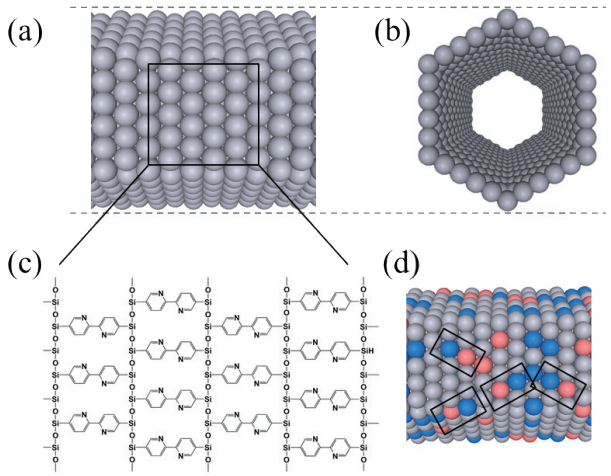

Fig. 7 Schematic images of model used in the Monte Carlo (MC) simulation: (a) model of a mesopore (side view), (b) model of a mesopore (front view), (c) correspondence between the model and the pore-wall structure of BPy-PMO, and (d) an example of a simulated structure. Some of the B spheres (gray) are replaced by P spheres (red) or C spheres (blue). P−C pairs are shown in rectangular boxes.

electron transfer from $[Ru(bpy)_3]^{2+}$ to $Re(bpy)(CO)_3Cl$ upon photoexcitation. A cluster model of Ru-Re-BPy-PMO (**Fig. 8**(a)) was prepared by utilizing molecular dynamics simulations and its electronic states were examined using quantum chemical calculations. The molecular orbitals that were relevant to the electron transfer were calculated using DFT with the B3LYP functional. See the supporting information of Ref. (20) for other calculation details. As shown in Fig. 8, the HOMO, LUMO and LUMO+1 are mainly distributed on Ru, the bpy ligand of the Re-complex and the bpy ligand of $[Ru(bpy)_3]^{2+}$ within

Table 3 N_P, N_C and N_{CP} values obtained by MC simulations for $Ru(PS)_x$-$Ru(Cat)_y$-BPy-PMO.

Run	Molar ratio[a]		Probability[b]		N_P	N_C	N_{CP}	N_{CP} (mmol g^{-1})[c]	TON[d]
	x	y	P	C					
1	0.040	0.073	0.060	0.1095	59476	109545	24854	0.079	15.3
2	0.040	0.034	0.060	0.051	59760	50979	11729	0.037	11.8
3	0.040	0.0031	0.060	0.0047	60068	4667	1049	0.003	3.8
4	0.110	0.065	0.165	0.0975	163926	97080	53581	0.171	24.0
5	0.110	0.038	0.165	0.0570	164863	56047	30906	0.099	21.7
6	0.110	0.0055	0.165	0.00825	164538	8318	4634	0.015	9.4

[a] Experimental conditions.
[b] Set to be 1.5 times greater than molar ratios. See also text.
[c] N_{CP} (mmol g^{-1}) = 3.18N_{CP}/996000. The molar concentration of bpy moieties in BPy-PMO is estimated to be 3.18 mmol g^{-1}.(18)
[d] Turnover number calculated by dividing the molar amount of products by the amount of Ru(Cat).

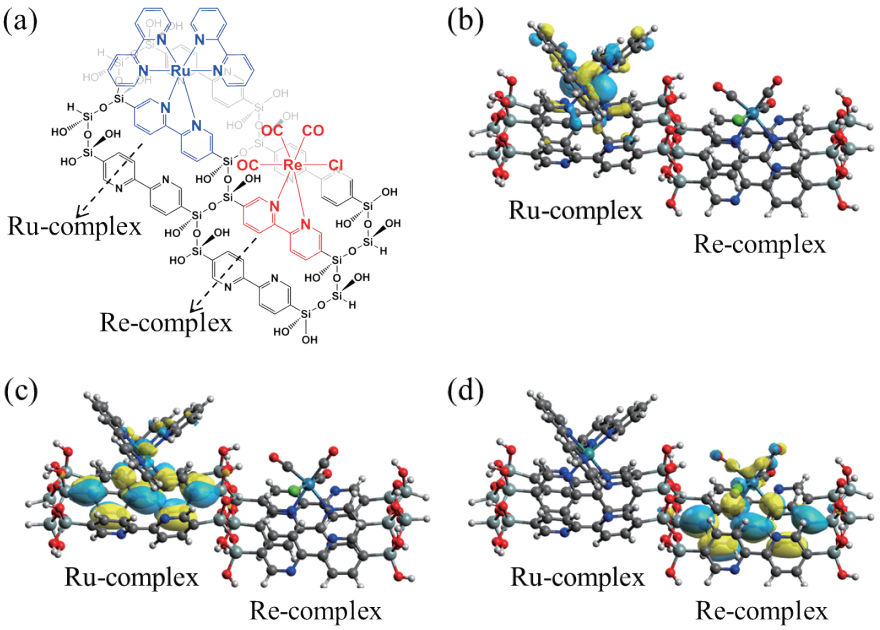

Fig. 8 Cluster model of a Ru-Re complex pair and their orbitals obtained by DFT with the B3LYP functional. (a) Model structure, (b) HOMO, (c) LUMO+1, and (d) LUMO.

the pore walls, respectively. It is noteworthy that the LUMO+1 and LUMO are also partially spread over Si−C and Si−O bonds that connect the two complexes. These orbitals suggest that the electron transfer proceeds as follows: (i) metal-to-ligand charge transfer (MLCT) excitation of $[Ru(bpy)_3]^{2+}$ by photoirradiation; (ii) consequently, one of the electrons in the HOMO transfers to the LUMO+1; and (iii) the electron tunnels from the LUMO+1 to LUMO through the Si−O−Si bond. The results indicate the possible presence of electronic interactions of the PMO organic groups through the silica framework in addition to the π−π interactions that have been previously focused on. A long range electron transfer between the complexes is hardly expected because the LUMO+1 and LUMO are only slightly distributed to the silica framework. Although the calculations suggest a through-bond electron transfer as noted above, further studies including an experimental approach are required to corroborate this contribution.

4. Summary

The PMO organic groups are densely introduced in the pore wall and are in proximity to each other. This unique structure induces intermolecular interactions of the organic groups that have significant potential to play central roles in the functionalities. In this article, our studies on excimer formation in the pore wall and the electron transfer between metal complexes formed on the pore surfaces are briefly reviewed.

The results of systematic calculations of typical aromatic dimers demonstrated that the excimer fluorescence energy could be accurately evaluated by incorporating both the contributions of the main configurations of the excimeric state and dynamical correlation into the computation. The calculations of cyclophane derivatives indicate that the electronic properties of the organic groups of PMO materials are dominated by transannular interactions and substituent effects of the silica framework. Large displacements of the aromatic rings from their original positions upon photoexcitation were also suggested. The distribution of metal complexes in Ru(Cat)-Ru(PS)-BPy-PMO was studied by MC simulations. The results suggested that a complex pair in which Ru(Cat) and Ru(PS) are connected by a Si−O−Si bond on the surface is the active center for CO_2 reduction photocatalysis. The complex pair of Ru-Re-BPy-PMO was modeled as a cluster and calculated by a quantum chemical method to reveal the mechanism of electron transfer between the two complexes. The results suggest that the electron transfers from Ru to the bpy organic group in $[Ru(bpy)_3]^{2+}$ and then tunnels to the bpy ligand of $Re(bpy)(CO)_3Cl$ through a Si−O−Si bond.

The intermolecular interactions of the organic groups are based on the atomistic-scale molecular structures and the wavefunction of the material, which are both difficult to be directly analyzed experimentally. Theoretical calculations enable visualization of these features and examination of the detailed mechanism that underlies the observed phenomena and functionalities. The interplay of theory and experiment is demonstrated here as becoming more essential in the study and development of functional PMO materials.

Acknowledgments

The studies on the excimer fluorescence of the PMO were supported by JST CREST. Prof. Suehiro Iwata, a visiting professor at Keio University and a former fellow at Toyota Physical and Chemical Research Institute, is also acknowledged for his great support on these studies. The studies on the electron transfer between the metal complexes on the BPy-PMO pore surfaces were supported by JST ACT-C Grant Number JPMJCR12Y1 and by JSPS KAKENHI Grant Number JP24107002.

References

(1) Inagaki, S., Guan, S., Fukushima, Y., Ohsuna, T. and Terasaki, O., “Novel Mesoporous Materials with a Uniform Distribution of Organic Groups and Inorganic Oxide in Their Frameworks”, *J. Am. Chem. Soc.*, Vol. 121, No. 41 (1999), pp. 9611-9614.

(2) Asefa, T., MacLachlan, M. J., Coombs, N. and Ozin, G. A., “Periodic Mesoporous Organosilicas with Organic Groups Inside the Channel Walls”, *Nature*, Vol. 402, No. 6764 (1999), pp. 867-871.

(3) Melde, B. J., Holland, B. T., Blanford, C. F. and Stein, A., “Mesoporous Sieves with Unified Hybrid Inorganic/Organic Frameworks”, *Chem. Mater.*, Vol. 11, No. 11 (1999), pp. 3302-3308.

(4) Yoshina-Ishii, C., Asefa, T., Coombs, N., MacLachlan, M. J. and Ozin, G. A., “Periodic Mesoporous Organosilicas, PMOs: Fusion of Organic and Inorganic Chemistry ‘Inside’ the Channel Walls of Hexagonal Mesoporous Silica”, *Chem. Commun.*, Vol. 24 (1999), pp. 2539-2540.

(5) Inagaki, S., Guan, S., Ohsuna, T. and Terasaki, O., "An Ordered Mesoporous Organosilica Hybrid Material with a Crystal-like Wall Structure", *Nature*, Vol. 416, No. 6878 (2002), pp. 304-307.
(6) Shea, K. J., Loy, D. A. and Webster, O., "Arylsilsesquioxane Gels and Related Materials. New Hybrids of Organic and Inorganic Networks", *J. Am. Chem. Soc.*, Vol. 114, No. 17 (1992), pp. 6700-6710.
(7) Corriu, R. J. P., "Ceramics and Nanostructures from Molecular Precursors", *Angew. Chem., Int. Ed.*, Vol. 39, No. 8 (2000), pp. 1376-1398.
(8) Loy, D. A. and Shea, K. J., "Bridged Polysilsesquioxanes. Highly Porous Hybrid Organic-inorganic Materials", *Chem. Rev.*, Vol. 95, No. 5 (1995), pp. 1431-1442.
(9) Fujita, S. and Inagaki, S., "Self-organization of Organosilica Solids with Molecular-scale and Mesoscale Periodicities", *Chem. Mater.*, Vol. 20, No. 3 (2008), pp. 891-908.
(10) Mizoshita, N., Tani, T. and Inagaki, S., "Syntheses, Properties and Applications of Periodic Mesoporous Organosilicas Prepared from Bridged Organosilane Precursors", *Chem. Soc. Rev.*, Vol. 40, No. 2 (2011), pp. 789-800.
(11) Goto, Y., Mizoshita, N., Ohtani, O., Okada, T., Shimada, T., Tani, T. and Inagaki, S., "Synthesis of Mesoporous Aromatic Silica Thin Films and Their Optical Properties", *Chem. Mater.*, Vol. 20, No. 13 (2008), pp. 4495-4498.
(12) Mizoshita, N., Goto, Y., Tani, T. and Inagaki, S., "Highly Fluorescent Mesostructured Films That Consist of Oligo(Phenylenevinylene)–silica Hybrid Frameworks", *Adv. Funct. Mater.*, Vol. 18, No. 22 (2008), pp. 3699-3705.
(13) Inagaki, S., Ohtani, O., Goto, Y., Okamoto, K., Ikai, M., Yamanaka, K., Tani, T. and Okada, T., "Light Harvesting by a Periodic Meoporous Organosilica Chromophore", *Angew. Chem., Int. Ed.*, Vol. 48, No. 22 (2009), pp. 4042-4046.
(14) Yamanaka, K., Okada, T., Goto, Y., Tani, T. and Inagaki, S., "Dynamics in the Excited Electronic State of Periodic Mesoporous Biphenylylene-silica Studied by Time-resolved Diffuse Reflectance and Fluorescence Spectroscopy", *Phys. Chem. Chem. Phys.*, Vol. 12, No. 37 (2010), pp. 11688-11696.
(15) Yamanaka, K., Okada, T., Goto, Y., Ikai, M., Tani, T. and Inagaki, S., "Dynamics of Excitation Energy Transfer from Biphenylylene Excimers in Pore Walls of Periodic Mesoporous Organosilica to Coumarin 1 in the Mesochannels", *J. Phys. Chem. C*, Vol. 117, No. 28 (2013), pp. 14865-14871.
(16) Mizoshita, N., Ikai, M., Tani, T. and Inagaki, S., "Hole-transporting Periodic Mesostructured Organosilica", *J. Am. Chem. Soc.*, Vol. 131, No. 40 (2009), pp. 14225-14227.
(17) Ikai, M., Maegawa, Y., Goto, Y., Tani, T. and Inagaki, S., "Synthesis of Visible-light-absorptive and Hole-transporting Periodic Mesoporous Organosilica Thin Films for Organic Solar Cells", *J. Mater. Chem. A*, Vol. 2, No. 30 (2014), pp. 11857-11865.
(18) Waki, M., Maegawa, Y., Hara, K., Goto, Y., Shirai, S., Yamada, Y., Mizoshita, N., Tani, T., Chun, W.-J., Muratsugu, S., Tada, M., Fukuoka, A. and Inagaki, S., "A Solid Chelating Ligand: Periodic Mesoporous Organosilica Containing 2,2'-bipyridine within the Pore Walls.", *J. Am. Chem. Soc.*, Vol. 136, No. 10 (2014), pp. 4003-4011.
(19) Kuramochi, Y., Sekine, M., Kitamura, K., Maegawa, Y., Goto, Y., Shirai, S., Inagaki, S. and Ishida, H., "Photocatalytic CO_2 Reduction by Periodic Mesoporous Organosilica (PMO) Containing Two Different Ruthenium Complexes as Photosensitizing and Catalytic Sites", *Chem. - Eur. J.*, Vol. 23, No. 43 (2017), pp. 10301-10309.
(20) Waki, M., Yamanaka, K., Shirai, S., Maegawa, Y., Goto, Y., Yamada, Y. and Inagaki, S., "$Re(bpy)(CO)_3Cl$ Immobilized on Bipyridine-periodic Mesoporous Organosilica for Photocatalytic CO_2 Reduction", *Chem. - Eur. J.*, Vol. 24, No. 15 (2018), pp. 3846-3853.
(21) Takeda, H., Goto, Y., Maegawa, Y., Ohsuna, T., Tani, T., Matsumoto, K., Shimada, T. and Inagaki, S., "Visible-light-harvesting Periodic Mesoporous Organosilica", *Chem. Commun.*, Vol. 40 (2009), pp. 6032-6034.
(22) Takeda, H., Ohashi, M., Tani, T., Ishitani, O. and Inagaki, S., "Enhanced Photocatalysis of Rhenium(I) Complex by Light-harvesting Periodic Mesoporous Organosilica", *Inorg. Chem.*, Vol. 49, No. 10 (2010), pp. 4554-4559.
(23) Yui, T., Takeda, H., Ueda, Y., Sekizawa, K., Koike, K., Inagaki, S. and Ishitani, O., "Hybridization Between Periodic Mesoporous Organosilica and a Ru(II) Polypyridyl Complex with Phosphonic Acid Anchor Groups", *ACS Appl. Mater. Interfaces*, Vol. 6, No. 3 (2014), pp. 1992-1998.
(24) Yamamoto, Y., Takeda, H., Yui, T., Ueda, Y., Koike, K., Inagaki, S. and Ishitani, O., "Efficient Light Harvesting via Sequential Two-step Energy Accumulation Using a Ru–Re_5 Multinuclear Complex Incorporated into Periodic Mesoporous Organosilica", *Chem. Sci.*, Vol. 5, No. 2 (2014), pp. 639-648.
(25) Förster, T. and Kasper, K., "Ein Konzentrationsumschlag der Fluoreszenz", *Z. Phys. Chem.*, Vol. 1, No. 5-6 (1954), pp. 275-277.
(26) Shirai, S., Iwata, S., Tani, T. and Inagaki, S., "Ab Initio Studies of Aromatic Excimers Using Multiconfiguration Quasi-degenerate Perturbation Theory", *J. Phys. Chem. A*, Vol. 115, No. 26 (2011), pp. 7687-7699.

(27) Shirai, S., Iwata, S., Maegawa, Y., Tani, T. and Inagaki, S., "Ab Initio Molecular Orbital Study on the Excited States of [2.2]-, [3.3]-, and Siloxane-bridged Paracyclophanes", *J. Phys. Chem. A*, Vol. 116, No. 41 (2012), pp. 10194-10202.
(28) Förster, T., "Excimers", *Angew. Chem., Int. Ed.*, Vol. 8, No. 5 (1969), pp. 333-343.
(29) Scholes, G. D. and Ghiggino, K. P., "Electronic Interactions and Interchromophore Excitation Transfer", *J. Phys. Chem.*, Vol. 98, No. 17 (1994), pp. 4580-4590.
(30) Nakano, H., "Quasidegenerate Perturbation Theory with Multiconfigurational Self-consistent-field Reference Functions", *J. Chem. Phys.*, Vol. 99, No. 10 (1993), pp. 7983-7992.
(31) Becke, A. D., "Density-functional Thermochemistry. III. The Role of Exact Exchange", *J. Chem. Phys.*, Vol. 98, No. 7 (1993), pp. 5648-5652.
(32) Stephens, P. J., Devlin, F. J., Chabalowski, C. F. and Frisch, M. J., "Ab Initio Calculation of Vibrational Absorption and Circular Dichroism Spectra Using Density Functional Force Fields", *J. Phys. Chem.*, Vol. 98, No. 45 (1994), pp. 11623-11627.
(33) Frisch, M. J., Trucks, G. W., Schlegel, H. B., Scuseria, G. E., Robb, M. A., Cheeseman, J. R., Montgomery, Jr., J. A., Vreven, T., Kudin, K. N., Burant, J. C., Millam, J. M., Iyengar, S. S., Tomasi, J., Barone, V., Mennucci, B., Cossi, M., Scalmani, G., Rega, N., Petersson, G. A., Nakatsuji, H., Hada, M., Ehara, M., Toyota, K., Fukuda, R., Hasegawa, J., Ishida, M., Nakajima, T., Honda, Y., Kitao, O., Nakai, H., Klene, M., Li, X., Knox, J. E., Hratchian, H. P., Cross, J. B., Bakken, V., Adamo, C., Jaramillo, J., Gomperts, R., Stratmann, R. E., Yazyev, O., Austin, A. J., Cammi, R., Pomelli, C., Ochterski, J. W., Ayala, P. Y., Morokuma, K., Voth, G. A., Salvador, P., Dannenberg, J. J., Zakrzewski, V. G., Dapprich, S., Daniels, A. D., Strain, M. C., Farkas, O., Malick, D. K., Rabuck, A. D., Raghavachari, K., Foresman, J. B., Ortiz, J. V., Cui, Q., Baboul, A. G., Clifford, S., Cioslowski, J., Stefanov, B. B., Liu, G., Liashenko, A., Piskorz, P., Komaromi, I., Martin, R. L., Fox, D. J., Keith, T., Al-Laham, M. A., Peng, C. Y., Nanayakkara, A., Challacombe, M., Gill, P. M. W., Johnson, B., Chen, W., Wong, M. W., Gonzalez, C. and Pople, J. A., *Gaussian 03, Revision E. 01* (2004), Gaussian, Inc., Wallingford CT.
(34) Schmidt, M. W., Baldridge, K. K., Boatz, J. A., Elbert, S. T., Gordon, M. S., Jensen, J. H., Koseki, S., Matsunaga, N., Nguyen, K. A., Su, S., Windus, T. L., Dupuis, M. and Montgomery Jr., J. A., "General Atomic and Molecular Electronic Structure System", *J. Comput. Chem.*, Vol. 14, No. 11 (1993), pp. 1347-1363.
(35) Hehre, W. J., Ditchfield, R. and Pople, J. A., "Self-consistent Molecular Orbital Methods. XII. Further Extensions of Gaussian-type Basis Sets for Use in Molecular Orbital Studies of Organic Molecules", *J. Chem. Phys.*, Vol. 56, No. 5 (1972), pp. 2257-2261.
(36) Hariharan, P. C. and Pople, J. A., "The Influence of Polarization Functions on Molecular Orbital Hydrogenation Energies", *Theor. Chim. Acta*, Vol. 28, No. 3 (1973), pp. 213-222.
(37) Azumi, T. and McGlynn, S. P., "Energy of Excimer Luminescence. I. A Reconsideration of Excimer Processes", *J. Chem. Phys.*, Vol. 41, No. 10 (1964), pp. 3131-3138.
(38) Hiraya, A. and Shobatake, K., "Direct Absorption Spectra of Jet-cooled Benzene in 130–260 nm", *J. Chem. Phys.*, Vol. 94, No. 12 (1991), pp. 7700-7706.
(39) George, G. A. and Morris, G. C., "The Intensity of Absorption of Naphthalene from 30000 cm^{-1} to 53000 cm^{-1}", *J. Mol. Spectrosc.*, Vol. 26, No. 1 (1968), pp. 67-71.
(40) McVey, J. K., Shold, D. M. and Yang, N. C., "Direct Observation and Characterization of Anthracene Excimer in Solution", *J. Chem. Phys.*, Vol. 65, No. 8 (1976), pp. 3375-3376.
(41) Katoh, R., Sinha, S., Murata, S. and Tachiya, M., "Origin of the Stabilization Energy of Perylene Excimer as Studied by Fluorescence and Near-IR Transient Absorption Spectroscopy", *J. Photochem. Photobiol. A*, Vol. 145, No. 1-2 (2001), pp. 23-34.
(42) Shirai, S., Kurashige, Y. and Yanai, T., "Computational Evidence of Inversion of ^1L_a and ^1L_b-derived Excited States in Naphthalene Excimer Formation from Ab Initio Multireference Theory with Large Active Space: DMRG-CASPT2 Study", *J. Chem. Theory Comput.*, Vol. 12, No. 5 (2016), pp. 2366-2372.
(43) Huenerbein, R. and Grimme, S., "Time-dependent Density Functional Study of Excimers and Exciplexes of Organic Molecules", *Chem. Phys.*, Vol. 343, No. 2-3 (2008), pp. 362-371.
(44) Cram, D. J., Allinger, N. L. and Steinberg, H., "Macro Rings. VII. The Spectral Consequences of Bringing Two Benzene Rings Face to Face", *J. Am. Chem. Soc.*, Vol. 76, No. 23 (1954), pp. 6132-6141.
(45) Iwata, S., Fuke, K., Sasaki, M., Nagakura, S., Otsubo, T. and Misumi, S., "Electronic Spectra and Electronic Structures of [2.2]Paracyclophane and Related Compounds", *J. Mol. Spectrosc.*, Vol. 46, No.1 (1973), pp. 1-15.
(46) Winnik, F. M., "Photophysics of Preassociated Pyrenes in Aqueous Polymer Solutions and in Other Organized Media", *Chem. Rev.*, Vol. 93, No. 2 (1993), pp. 587-614.

(47) Yamaji, M., Tsukada, T., Shizuka, H. and Nishimura, J., "Synthesis of a [3.3]Biphenylophane, and Its Photophysical and Photochemical Properties Studied by Emission and Transient Absorption Measurements", *Chem. Phys. Lett.*, Vol. 460, No. 4-6 (2008), pp. 474-477.
(48) Yamaji, M., Okamoto, H., Hakoshima, Y. and Shinmyozu, T., "Photophysical and Photochemical Processes of Excited Singlet and Triplet [3_n]Cyclophanes (n = 2–6) Studied by Emission Measurements and Steady-state and Laser Flash Photolyses", *J. Phys. Chem. A*, Vol. 119, No. 10 (2015), pp. 1867-1874.
(49) Francl, M. M., Pietro, W. J., Hehre, W. J., Binkley, J. S., Gordon, M. S., DeFrees, D. J. and Pople, J. A., "Self-consistent Molecular Orbital Methods. XXIII. A Polarization-type Basis Set for Second-row Elements", *J. Chem. Phys.*, Vol. 77, No. 7 (1982), pp. 3654-3665.

Soichi Shirai
Research Field:
- Quantum Chemical Calculations of Molecules and Materials

Academic Degree: Dr.Sci.
Academic Societies:
- The Chemical Society of Japan
- Japan Society for Molecular Science
- The Japanese Association of Theoretical Chemists
- American Chemical Society